
# 3D printing of drug-loaded gyroid lattices using selective laser sintering

Fabrizio Fina, Alvaro Goyanes, Christine M. Madla, Atheer Awad, Sarah J. Trenfield, Jia Min Kuek, Pavanesh Patel, Simon Gaisford, Abdul W. Basit

PII: S0378-5173(18)30354-5
DOI: https://doi.org/10.1016/j.ijpharm.2018.05.044
Reference: IJP 17515

To appear in: *International Journal of Pharmaceutics*

Received Date: 5 March 2018
Revised Date: 17 May 2018
Accepted Date: 18 May 2018

Please cite this article as: F. Fina, A. Goyanes, C.M. Madla, A. Awad, S.J. Trenfield, J.M. Kuek, P. Patel, S. Gaisford, A.W. Basit, 3D printing of drug-loaded gyroid lattices using selective laser sintering, *International Journal of Pharmaceutics* (2018), doi: https://doi.org/10.1016/j.ijpharm.2018.05.044

# 3D printing of drug-loaded gyroid lattices using selective laser sintering

Fabrizio Fina[1], Alvaro Goyanes[2]*, Christine M Madla[1], Atheer Awad[1], Sarah J. Trenfield[1], Jia Min Kuek[1], Pavanesh Patel[1], Simon Gaisford[1, 2], Abdul W Basit[1, 2]*

[1]Department of Pharmaceutics, UCL School of Pharmacy, University College London, 29-39 Brunswick Square, London WC1N 1AX, UK

[2]FabRx Ltd., 3 Romney Road, Ashford, Kent, TN24 0RW, UK

*Correspondence: Abdul W. Basit - a.basit@ucl.ac.uk

Alvaro Goyanes - a.goyanes@FabRx.co.uk

**Abstract**

Three-dimensional printing (3DP) is gaining momentum in the field of pharmaceuticals, offering innovative opportunities for medicine manufacture. Selective laser sintering (SLS) is a novel, high resolution and single-step printing technology that we have recently introduced to the pharmaceutical sciences. The aim of this work was to use SLS 3DP to fabricate printlets (3D printed tablets) with cylindrical, gyroid lattice and bi-layer structures having customisable release characteristics. Paracetamol-loaded constructs from four different pharmaceutical grade polymers, including polyethylene oxide, Eudragit (L100-55 and RL) and ethyl cellulose, were created using SLS 3DP. The novel gyroid lattice structure was employed to modulate the drug release from all four polymers. This work is the first to demonstrate the feasibility of using SLS to achieve customised drug release properties of several polymers, in a swift, cost-effective process, avoiding the need to alter the formulation composition. As such, by creating these constructs, it is possible to modify drug release, which in practice could enable the tailoring of drug performance to the patient simply by changing the 3D design.

Keywords:

rapid prototyping; additive manufacturing; personalized medicines; acrylic polymers; fused deposition modeling (FDM); stereolithography (SLA).

## 1. Introduction

The most common pharmaceutical manufacturing processes were first introduced almost 200 years ago. The use of these traditional techniques, from powder compaction to encapsulation, limit solid oral dosage forms to formulations with conventional structures. The introduction of three-dimensional printing (3DP) to the pharmaceutical sciences, however, has the potential to cause a paradigm shift in medicine manufacture (Trenfield et al., 2018) and create dosage forms and tailor drug doses individualised to the needs of the patient (Alhnan et al., 2016; Alomari et al., 2015; Choonara et al., 2016; Goyanes et al., 2017a; Goyanes et al., 2017b).

3D printing has a number of pharmaceutical applications, ranging from the manufacture of orodispersible tablets using binder jet printing technology (Pharmaceutials, 2015), medical devices (Bloomquist et al., 2018), donut-shaped tablets (Wang et al., 2016), drug-loaded hydrogels using stereolithography (SLA) (Martinez et al., 2017), polypills incorporating 5 drugs using semisolid extrusion (Khaled et al., 2015a; Khaled et al., 2015b), to the fabrication of channelled tablets (Sadia et al., 2018), mini capsules (Goyanes et al., 2018), capsules incorporating liquids (Okwuosa et al., 2018), printlets loaded with nanocapsules (Beck et al., 2017), duocaplets using fused-deposition modelling (FDM) (Goyanes et al., 2015c). However, these technologies are associated with a number of challenges. For instance, binder jet technology generates prints of low mechanical strength, SLA requires the use of non-pharma grade materials and semisolid extrusion suffers from low resolution, whilst the most investigated printing technology FDM (Genina et al., 2017; Melocchi et al., 2015; Melocchi et al., 2016) is generally associated with elevated printing temperatures (Goyanes et al., 2015a; Goyanes et al., 2016a; Kollamaram et al., 2018; Okwuosa et al., 2016).

Selective laser sintering (SLS) is a relatively new 3DP technology that offers innovative opportunities to the scope of medicine manufacture. This technique functions by utilising a laser beam that selectively sinters powder particles together, allowing the fabrication of highly detailed structures. As such, tuneable release profiles, ranging from immediate (Fina et al., 2018) to modified (Fina et al., 2017) release can be easily attained. In addition, as the unsintered powder remains loose and could be reused, it minimises the wastage of material and promotes recycling of the feedstock. Moreover, this highlights the cost–effectiveness of

the technology; in a comparison between technologies, SLS was found to be more economical than FDM, SLA and injection moulding (Hopkinson and Dicknes, 2003).

3D printed oral solid dosage forms fabricated to date using other technologies have shown a multitude of designs and forms, however the use of SLS would allow the construction of previously difficult to manufacture structures from pharmaceutical grade excipients. As such, we aimed to create structures termed 3D gyroid lattice constructs. They are porous solids that can be manufactured with a broad range of micro-structures and length scales (Khaderi et al., 2014). These constructs, which can be random or periodic and designed with an open or closed cell, are often explored in engineering to modify the properties of the object (Yan et al., 2012). By adapting this geometry to pharmaceutical use, the integration of open cells can increase the amount of drug in superficial layers, enhancing its contact and exposure to the dissolution media, and consequently facilitating its release.

The aim of this study was to explore SLS as a suitable 3DP technique to fabricate novel gyroid lattice structures using four different polymers and investigate their feasibility to be exploited for the tailoring of drug performance based on individual patients' needs. As such, they could be utilised to alter the drug release characteristics of oral products while keeping the formulation composition constant.

## 2. Materials and methods

### *2.1. Materials*

Paracetamol USP grade (Sigma-Aldrich, UK) was used as a model drug (MW 151.16, solubility at 37ºC: 21.80 g/L. Eudragit L100-55, a copolymer of methacrylic acid and ethyl acrylate (1:1 ratio) that dissolves at pH 5.5 and above and Eudragit RL (copolymer of ethyl acrylate, methyl methacrylate and a low content of methacrylic acid ester with quaternary ammonium groups: the ammonium groups present as salts making the polymer permeable) were kindly donated by Evonik, Germany. Ethyl cellulose N7 (ethoxyl-grade N, ethoxyl content 48.0-49.5%, viscosity 5.6-8 mPa•s) was kindly donated by Hercules, US. Polyethylene oxide (PEO 1,000,000 MW; PEO 1M) (WSR N-12K LEO NF) was kindly donated by Colorcon, UK. Candurin® Gold Sheen was purchased from Azelis, UK. The salts for preparing the buffer dissolution media were purchased from VWR International Ltd., UK.

### *2.2 Methods*

#### *2.2.1. Design of the formulations*

The software AutoCAD 2014 (Autodesk Inc., USA) was used to design the templates of the cylindrical printlets, size 10mm diameter x 3.6mm height (Figure 1A). The software Functional Lattice Package for Additive Manufacturing (Flatt Pack v1.4, Added Scientific, UK) used for generating surface lattices into components was used to generate the novel lattice structured printlets (Figure 1B). The software offers optimisation algorithms to enable increased product performance of 3D printed objects by changing the internal lattice structure. For the printlets, the design parameters were set as follows: the geometry selected was a cylinder with dimensions X: 10 mm, Y: 10 mm and Z: 3.6 mm; number of cells X: 3, Y: 3, Z: 2; the cell type selected was a gyroid with a network phase; value of uniform density 0.2; No skin was selected and the STL triangle reduction value was 0.2.

Additionally, a bi-layer model, compromising cylindrical and lattice fragments, was designed with the following parameters: the cylindrical portion was X: 10 mm, Y: 10 mm and Z: 1.44 mm. The lattice portion was X: 10 mm, Y: 10 mm and Z: 2.16 mm; number of cells X: 3, Y: 3, Z: 1. The remaining parameters were kept the same as the gyroid lattice printlets. All the 3D models of the cylindrical, lattice and bi-layer constructs were exported as a stereolithography (.stl) file into the 3D printer Sintratec central software Version 1.1.13.

#### *2.2.2. Printing process*

For all the formulations, 100g of a mixture of drug and excipients were blended using a mortar and pestle (Table 1). To ensure that a suitable particle size was obtained for printing, the ethyl cellulose and polyethylene oxide powders were sieved using a 180μm sieve prior to their mixing with the other excipients. 3% of Candurin® Gold Sheen was added to all the formulations to enhance energy absorption from the laser and allow printability. Powder mixtures were transferred to a desktop SLS printer (Sintratec Kit, AG, Brugg, Switzerland) to fabricate the oral dosage formulations. Powder in the platform reservoir (150x150x150 mm) of the printer was moved by a sled to a building platform (150x150x150 mm) creating a flat and homogeneously distributed layer of powder. The printing surface temperatures

ranged from 50°C to 120°C. The 2.3W blue diode laser (445nm) was activated to sinter the powder on the building platform in a certain pattern based on the .stl file. At this point, the reservoir platform moved up, the building platform moved down, and the sled distributed a thin layer of powder on top of the previous layer. This process was repeated layer-by-layer until the object was completed. Printlets were then removed from the powder bed and the excess powder was brushed off. Ten printlets were printed at the same time for each formulation. In addition, bi-layer printlets compromising a combination of gyroid lattice and cylindrical constructs were fabricated using the PEO mixture, wherein the same printing parameters were utilised.

### *2.3. Thermal analysis*

Differential scanning calorimetry (DSC) was used to characterise the powders and the drug loaded printlets. DSC measurements were performed with a Q2000 DSC (TA instruments, Waters, LLC, USA) at a heating rate of 10°C/min. Calibration for cell constant and enthalpy was performed with indium (Tm = 156.6°C, ΔHf =28.71J/g) according to the manufacturer instructions. Nitrogen was used as a purge gas with a flow rate of 50mL/min for all the experiments. Data were collected with TA Advantage software for Q series (version 2.8.394), and analysed using TA Instruments Universal Analysis 2000. All melting temperatures are reported as extrapolated onset unless otherwise stated. TA aluminium pans and lids (Tzero) were used with an average sample mass of 8-10 mg.

### *2.4. X-ray powder diffraction (XRPD)*

Discs of 23mm diameter x 1mm height made from the mixtures of drug and excipients were 3D printed and analysed. Samples of pure paracetamol and the mixtures were also analysed. The X-ray powder diffraction patterns were obtained in a Rigaku MiniFlex 600 (Rigaku, USA) using a Cu Kα X-ray source (λ=1.5418Å). The intensity and voltage applied were 15mA and 40kV. The angular range of data acquisition was 3–60° 2θ, with a stepwise size of 0.02° at a speed of 5°/min.

### *2.5. Characterisation of the printlets*

#### *2.5.1. Determination of printlet morphology*

The diameter and thickness of the printlets were measured using a digital calliper. Images were captured with a camera Sony α6300.

### *2.5.2. Scanning Electron Microscopy (SEM)*

Surface and cross-section images of the printlets were taken with a scanning electron microscope (SEM, JSM-840A Scanning Microscope, JEOL GmbH, Germany). All samples for SEM testing were coated with carbon (~30–40nm).

### *2.5.3. X-ray Micro Computed Tomography (Micro-CT)*

A high-resolution X-ray micro computed tomography scanner (SkyScan1172, Bruker-microCT, Belgium) was used to 3D visualise the internal structure, density and porosity of the printlets. All oral formulations were scanned with a resolution of 2000x1048 pixels. 3D imaging was performed by rotating the object through 180° with steps of 0.4° and four images were recorded for each of those. Image reconstruction was performed using NRecon software (version 1.7.0.4, Bruker-microCT). 3D model rendering and viewing were performed using the associate program CT-Volume (CTVol version 2.3.2.0) software. The collected data was analysed using the software CT Analyzer (CTan version 1.16.4.1). Porosity values for all the printlets were calculated using the 3D analysis in the morphometry preview. Specifically, 200 layers were selected at the central part of the printlets as area of interest and analysed. Additionally, the porosity of the lattice printlets was calculated as a mean of ten different individual sections at different heights of the printed structures with or without including non-printed spaces (openings) in the selection.

### *2.5.4. Determination of mechanical properties*

The breaking forces of six printlets of each formulation, in the cylindrical and lattice forms, were measured using a traditional tablet hardness tester TBH 200 (Erweka GmbH, Heusenstamm, Germany), whereby an increasing force, perpendicular to the printlet axis, was applied on its opposite sides, until the printlet fractured.

### *2.5.5. Determination of drug content*

Three finely crushed printlets of each polymer formulation were placed in separate volumetric flasks and filled with 250 mL deionised water. Ethyl cellulose-based printlets, however, were dissolved in ethanol as they were completely water insoluble. 4 drops of NaOH were added to the volumetric flasks containing Eudragit L100-55 based printlets in order to achieve a pH value of 5.5 and above. Samples of the solutions were then filtered through 0.45µm filters (Millipore Ltd., Ireland). The concentrations of drug determined were conducted using high performance liquid chromatography (HPLC, Hewlett Packard 1050

Series HPLC system, Agilent Technologies, UK). The validated HPLC assay involved injecting 20µL samples for analysis using a mobile phase consisted of methanol (15%) and water (85%) and passed through an Ultra C8 5µm column, 25 x 4.6mm (Restek, USA) maintained at 40°C. The mobile phase was pumped at a flow rate of 1 mL/min and the eluent was screened at a wavelength of 247nm.

#### *2.5.6. Dynamic dissolution testing conditions*

Drug dissolution profiles for the formulations were obtained with a USP-II apparatus (Model PTWS, Pharmatest, Germany) as follows; 1) the formulations were placed in 750 mL of 0.1M HCl for 2h to simulate gastric residence time; 2) transferred into 950 mL of modified Hanks (mHanks) bicarbonate physiological medium for 35min (pH 5.6 to 7); 3) and further transferred to 1000 mL of modified Krebs buffer (pH 7 to 7.4 and then to 6.5). The modified Hanks buffer based dissolution medium(Liu et al., 2011) (136.9mM NaCl, 5.37mM KCl, 0.812mM $MgSO_4.7H_2O$, 1.26mM $CaCl_2$, 0.337mM $Na_2HPO_4.2H_2O$, 0.441mM $KH_2PO_4$, 4.17mM $NaHCO_3$) forms an *in-situ* modified Kreb's buffer (Fadda and Basit, 2005) by the addition of 50 mL of pre-Krebs solution (400.7mM $NaHCO_3$ and 6.9mM $KH_2PO_4$) to each dissolution vessel.

The formulations were tested in the small intestinal environment for 3.5h (pH 5.6 to 7.4), followed by pH 6.5 representing colonic conditions (Fadda and Basit, 2005; Goyanes et al., 2015b; Liu et al., 2011; Varum et al., 2014). The medium is primarily a bicarbonate buffer in which bicarbonate ($HCO_3^-$) and carbonic acid ($H_2CO_3$) co-exist in equilibrium, along with aqueous carbon dioxide ($CO_2$, aq) resulting from dissociation of carbonic acid. The pH of the buffer is controlled by an Auto pH System$^{TM}$ (Merchant et al., 2012; Merchant et al., 2014), which consists of a pH probe connected to a source of $CO_2$ gas (pH-reducing gas), as well as to a supply of helium (pH-increasing gas), controlled by a control unit. The control unit is able to provide a dynamically adjustable pH during testing (dynamic conditions) and to maintain a uniform pH value over the otherwise unstable bicarbonate buffer pH. The paddle speed of the USP-II was fixed at 50rpm and the tests were conducted at 37 +/-0.5°C (n=3).

## 3. Results and Discussion

The four different powder mixtures were prepared using 92% polymer, 5% paracetamol and 3% Candurin® gold sheen (Table 1). The SLS technology fuses powder particles together using a thermal binding process (Shirazi et al., 2015). The laser beam traces the 3D design by drawing a pattern on the powder bed. As the temperature settles between the melting temperature ($T_m$) of the material and the $T_m/2$, a solid-state sintering occurs, leading to the partial binding of the powder particles. By finding the correct balance between the internal temperature of the printer and the laser scanning speed, it is possible to establish parameters suitable for printing (Table 1). By reducing the laser scanning speed, a longer interaction time between the powder particles and the laser beam leads to higher transmission of energy producing denser objects. Increasing the laser scanning speed, however, results in less energy being transmitted and thus weaker and more porous objects are produced.

Cylindrical and gyroid lattice constructs were successfully produced, expanding the number of pharmaceutical excipients that can be used with this technology (Figure 2). All the printlets were yellow due to the Candurin colourant. Candurin is an approved pharmaceutical excipient used in tablet coating; it was included into the drug and polymer mixtures at 3% w/w to facilitate the sintering process because it absorbs radiation at the wavelength of the laser (445 nm) (Fina et al., 2017).

SLS demonstrates two clear advantages to manufacture drug products with complex designs. Firstly; the laser employed in the present SLS printer allows the creation of extremely precise structures with the resolution of the printer being dependent on the laser and the powder particle size. Secondly; there is no need to print a support to sustain the object during the printing process. In SLS, the unsintered powder acts as a support itself which prevents the structure from collapsing. When the printing process is complete, the unsintered powder can be simply removed by air brushing or sieving. With other printing technologies such as FDM or SLA, a support is essential to produce suspended structures, which can potentially cause shape irregularity and/or dose inaccuracy upon removal. (Goyanes et al., 2016a).

The PEO printlets had a lower apparent density compared to the other formulations. The lattice EUD RL and PEO printlets showed ~ 3 fold lower apparent density than the cylindrical printlets, whilst the remaining formulations were only ~ 2 fold lower compared to their corresponding cylindrical printlets (Table 2). The PEO printlets were pliable and flattened during the breaking force test. As a consequence, the hardness testing equipment

could not detect a breaking force value for either the cylindrical or lattice printlets. The three other cylindrical printlets were strong, displaying similar breaking forces of ~ 280N. The lattice printlets of EUD L and EC were more friable and had lower breaking force values (~ 15N). The lattice printlets of EUD RL broke into small pieces during the analysis, thus, it was not possible to determine their breaking force value.

X-ray micro-CT was used to visualise the 3D structures of the cylindrical (Figure 3A) and novel lattice printlets (Figure 3B). This technique was further used to calculate the total porosity of the constructs (Table 2). It should be noted that herein the porosity refers to void spaces in the printlets and is a fraction of the volume of voids over the total volume as a percentage between 0 and 100%. Whereas openings refer to the non-printed spaces in the lattice constructs. For the lattice constructs, two values were calculated, whereby one value was calculated for the structure as whole (with openings) and the other value was a mean of ten different individual sections at different heights, wherein the openings were omitted from the selection. The presence of the openings in the lattice printlets significantly increased the porosity (minimum by 14%) when compared to the cylindrical printlets. Particularly significant was the increased porosity of the EC lattice printlet compared to the cylindrical printlet, which showed a very low porosity (3.4%). In the case of EUD L, the porosity did not change significantly by creating the lattice structure, although in the cylindrical printlets, the porosity value was already high (26.9%).

SEM images of the printlets validate the X-ray micro-CT results and provide a visual confirmation of the sintering processes in the polymer formulations (Figure 4). For the cylindrical printlets prepared with PEO and EUD L, the selected printing parameters resulted in a low intensity sintering process, and thus, created empty spaces between the powder particles, as shown in Table 2. The suitable parameters for the fabrication of EC and EUD RL formulations, however, led to a more intense sintering process. This allowed the powder particles to undergo a greater degree of melting, indicated by the larger molten surface. The same effect can be observed in the 3D printed gyroid lattice constructs, where the spherical polymer particles can be distinctively observed on the surface of the PEO and EUD L 3D printed lattice formulations due to the lighter sintering process (Figure 4B). EC and EUD RL lattice printlets, however, presented molten areas indicating a more energetic sintering effect due to a stronger laser impact on the materials. The differences in the molten areas for the different polymers can be explained by the laser speed utilised during the sintering process.

In this study, the selected laser speed was chosen based on what was considered suitable for the sintering process. Nonetheless, it has been reported that different laser speeds can result in printlets having different porosity values and drug release properties (Fina et al., 2018).

The analysis of the drug content in the printlets showed that the values were in agreement with the theoretical drug loading (5%), confirming that no drug degradation occurred during the printing process (Table 2).

DSC and X-ray analysis of the drug, polymers and mixed materials prior to printing, and of the printlets, were performed to identify the drug phase state and the degree of drug incorporation in the polymers (Figures 5 and 6). Before printing, the DSC data showed that the paracetamol raw ingredient exhibited a melting endotherm at approximately 172°C, indicative of form I which melts at 168°C (Sibik et al., 2014). The DSC data of the printlets showed no evidence of a melting endotherm at approximately 168°C. This demonstrated that the drug is either molecularly dispersed within the polymer matrix as a solid dispersion or is dissolved in the polymer as the temperature increases during the DSC procedure. PEO 1M showed an evident endotherm at around 60-65°C, indicating that the polymer was in its crystalline state. The aforementioned endotherm was also present in the printed formulation of PEO, indicating that the printing process conducted at 50°C did not alter the crystalline structure of the polymer. For EUD L, EUD RL and EC, no peaks were observed for the powder polymers, physical mixtures or the printed formulations. Thus, indicating that the polymers exist in the amorphous form or melt at a higher temperature.

Corroborating with the results obtained by DSC, x-ray diffractograms of EUD L, EUD RL and EC demonstrated amorphous patterns in all the physical mixtures and 3D printed formulations (Figure 6). PEO on the other hand, showed a clear crystalline diffractogram for the powder mixture. The printed PEO formulations, however, showed less crystalline peaks, indicating that a part of the polymer may have converted into an amorphous state.

Drug dissolution characteristics of the printlets were tested using a dynamic *in vitro* model, which simulates gastric and intestinal conditions of the gastrointestinal tract (Goyanes et al., 2015b) (Figure 7). With regards to the dissolution profile of the cylindrical formulations, PEO released 60% of the drug within the first 2 hours, and the remaining 40% of drug was

released in the following 4–5 hours. Owing to the enteric properties of the polymer, only 17% paracetamol release was observed from EUD L cylindrical printlets in the first 2 hours of the dissolution model. Following acidic conditions, however, the EUD L formulation showed a faster drug release in intestinal conditions commencing at pH 5.5, leading to complete dissolution in approximately 12 hours. Since EC is a water insoluble polymer, only 7% of paracetamol was released in the first 8 hours from the cylindrical printlets (overall, only 20% drug was released in 24 hours). The differences in the drug release patterns between EUD L and EC can be attributed to the higher porosity values of EUD L. This suggests that a higher volume of water was able to penetrate into the EUD L printlets and thus, the contact area was enlarged, leading to the acceleration of paracetamol release. Eudragit RL is a water insoluble polymer, having high permeability properties. Following an initial burst release, its cylindrical printlets released 95% of the drug in 24 hours, at a constant rate.

With regards to the dissolution profiles of the gyroid lattice printlets (Figure 7B), an overall reduction in the duration of the dissolution was observed for all printlets. This can be attributed to the increase in the exposed surface area and the higher porosity values, although porosity values are not always related with dissolution rate, as shown in a previous study with PVA caplets prepared by FDM 3D printing (Goyanes et al., 2016b). For instance, the PEO 1M macromolecules are characterised by the presence of oxygen molecules in their chains. As such, when PEO 1M is exposed to water, hydrophilic and hydrophobic interactions are formed, wherein the water molecules create a sheath around the PEO 1M macromolecules (Hammouda et al., 2004). By increasing the exposed surface area, more water molecules were attracted, resulting in a faster gel erosion and leading to the rapid drug release. Consequently, the lattice PEO printlets dissolved completely within just 10 minutes. As for the EUD RL lattice printlets, the complete drug release was achieved within 120 minutes. This observation can be linked to the polymer's chemical structure, wherein the high concentration of quaternary ammonium ions results in a pH-independent swelling and fluid permeation, leading to a subsequent dissolution and outward diffusion of the drug molecules (Dillen et al., 2006). As a result, by increasing the contact surface and enhancing the polymer porosity, more fluids are capable of permeating into the polymer matrix, resulting in an accelerated effect. EUD L on the other hand, lacks ammonium groups and instead its dissolution is dependent upon the content of carboxylic groups in the chain. As a result, the drug release occurs through diffusion and surface erosion of the polymer. Thus, by increasing the contact surface, the dissolution effect is amplified. Hence, the lattice printlets of the EUD

L polymer did not exhibit enteric properties and released most of the drug in acid. Similarly, the dissolution of drugs through EC occurs through diffusion, whereby the drug molecules diffuse through the pores on the surface of the matrix. Therefore, together, the enlarged contact surface and the marked increase in the polymer porosity, prompted the diffusion of more drug molecules and as a consequence, the EC lattice printlets exhibited a drug release ~4 fold higher than that of the cylindrical printlets.

To investigate the feasibility of further fine tuning the drug release, a new bi-layer configuration, comprising a combination of the gyroid lattice and cylindrical designs, was created (Figure 8A) and 3D printed using the polymer PEO as an exemplar (Figure 8B). As such, with 3DP heading towards integration into pharmacy practice for the personalisation of medications based on patients' needs (immediate release, prolonged release or combined release), these constructs could be exploited to modulate the drug release from printlets, without having to change the formulation composition.

The bi-layer PEO construct exhibited an intermediate release behaviour between that of the lattice structured and conventional PEO printlets (Figure 9). This observation can be explained by the partial presence of the lattice fragment, permitting an immediate burst of 50% of the drug in 30 minutes, whereas a more sustained release of the remainder drug from the conventional fragment was observed over the following 4 hours.

The bi-layer configuration was chosen as a model representing a formulation with adapted drug release characteristics. However, the possible configuration choices are numerous. For instance, other bi-layer layouts or even multi-layered constructs can also be fabricated. Potentially, in a clinical setting, this system would permit the use of a single (and perhaps standardised) formulation, easing the quality control and preparative processes of extemporaneous formulations, which in practice can be used to tailor the drug release to a specific patient simply by changing the 3D design.

## 4.0. Conclusion

We have successfully demonstrated that by creating unique and complex gyroid lattice and bi-layer constructs, SLS 3DP is efficient in modulating the drug release profiles of different pharmaceutical polymers. As such, the selection of appropriate parameters, including the internal lattice structure geometry, dimensions and lattice cell size or density, permits the tailoring of drug behaviour. Ultimately, this concept can be adopted for the personalisation of drug performance based on patients' needs, wherein a singular standardised ink could be utilised, obviating the need for altering the formulation composition.

## References

Alhnan, M.A., Okwuosa, T.C., Sadia, M., Wan, K.W., Ahmed, W., Arafat, B., 2016. Emergence of 3D Printed Dosage Forms: Opportunities and Challenges. Pharm. Res. 33, 1817-1832.

Alomari, M., Mohamed, F.H., Basit, A.W., Gaisford, S., 2015. Personalised dosing: Printing a dose of one's own medicine. Int. J. Pharm. 494, 568-577.

Beck, R.C.R., Chaves, P.S., Goyanes, A., Vukosavljevic, B., Buanz, A., Windbergs, M., Basit, A.W., Gaisford, S., 2017. 3D printed tablets loaded with polymeric nanocapsules: An innovative approach to produce customized drug delivery systems. Int. J. Pharm. 528, 268-279.

Bloomquist, C.J., Mecham, M.B., Paradzinsky, M.D., Janusziewicz, R., Warner, S.B., Luft, J.C., Mecham, S.J., Wang, A.Z., DeSimone, J.M., 2018. Controlling release from 3D printed medical devices using CLIP and drug-loaded liquid resins. J. Control. Release. 278, 9-23.

Choonara, Y.E., du Toit, L.C., Kumar, P., Kondiah, P.P.D., Pillay, V., 2016. 3D-printing and the effect on medical costs: a new era? Expert review of pharmacoeconomics & outcomes research 16, 23-32.

Dillen, K., Vandervoort, J., Van den Mooter, G., Ludwig, A., 2006. Evaluation of ciprofloxacin-loaded Eudragit® RS100 or RL100/PLGA nanoparticles. Int. J. Pharm. 314, 72-82.

Fadda, H.M., Basit, A.W., 2005. Dissolution of pH responsive formulations in media resembling intestinal fluids: bicarbonate versus phosphate buffers. J. Drug Deliv. Sci. Tec. 15, 273-279.

Fina, F., Goyanes, A., Gaisford, S., Basit, A.W., 2017. Selective laser sintering (SLS) 3D printing of medicines. Int. J. Pharm. 529, 285-293.

Fina, F., Madla, C.M., Goyanes, A., Zhang, J., Gaisford, S., Basit, A.W., 2018. Fabricating 3D printed orally disintegrating printlets using selective laser sintering. Int. J. Pharm. 541, 101-107.

Genina, N., Boetker, J.P., Colombo, S., Harmankaya, N., Rantanen, J., Bohr, A., 2017. Anti-tuberculosis drug combination for controlled oral delivery using 3D printed compartmental dosage forms: From drug product design to in vivo testing. J. Control. Release. 268, 40-48.

Goyanes, A., Buanz, A.B., Hatton, G.B., Gaisford, S., Basit, A.W., 2015a. 3D printing of modified-release aminosalicylate (4-ASA and 5-ASA) tablets. Eur. J. Pharm. Biopharm. 89, 157-162.

Goyanes, A., Hatton, G.B., Merchant, H.A., Basit, A.W., 2015b. Gastrointestinal release behaviour of modified-release drug products: Dynamic dissolution testing of mesalazine formulations. Int. J. Pharm. 484, 103-108.

Goyanes, A., Wang, J., Buanz, A., Martinez-Pacheco, R., Telford, R., Gaisford, S., Basit, A.W., 2015c. 3D Printing of Medicines: Engineering Novel Oral Devices with Unique Design and Drug Release Characteristics. Mol. Pharm. 12, 4077-4084.

Goyanes, A., Det-Amornrat, U., Wang, J., Basit, A.W., Gaisford, S., 2016a. 3D scanning and 3D printing as innovative technologies for fabricating personalized topical drug delivery systems. J. Control. Release. 234, 41-48.

Goyanes, A., Kobayashi, M., Martinez-Pacheco, R., Gaisford, S., Basit, A.W., 2016b. Fused-filament 3D printing of drug products: Microstructure analysis and drug release characteristics of PVA-based caplets. Int. J. Pharm. 514, 290-295.

Goyanes, A., Fina, F., Martorana, A., Sedough, D., Gaisford, S., Basit, A.W., 2017a. Development of modified release 3D printed tablets (printlets) with pharmaceutical excipients using additive manufacturing. Int. J. Pharm. 527, 21-30.

Goyanes, A., Scarpa, M., Kamlow, M., Gaisford, S., Basit, A.W., Orlu, M., 2017b. Patient acceptability of 3D printed medicines. Int. J. Pharm. 530, 71-78.

Goyanes, A., Fernandez-Ferreiro, A., Majeed, A., Gomez-Lado, N., Awad, A., Luaces-Rodriguez, A., Gaisford, S., Aguiar, P., Basit, A.W., 2018. PET/CT imaging of 3D printed devices in the gastrointestinal tract of rodents. Int. J. Pharm. 536, 158-164.

Hammouda, B., Ho, D.L., Kline, S., 2004. Insight into Clustering in Poly(ethylene oxide) Solutions. Macromolecules 37, 6932-6937.

Hopkinson, N., Dicknes, P., 2003. Analysis of rapid manufacturing—using layer manufacturing processes for production. Proceedings of the Institution of Mechanical Engineers, Part C: Journal of Mechanical Engineering Science 217, 31-39.

Khaderi, S.N., Deshpande, V.S., Fleck, N.A., 2014. The stiffness and strength of the gyroid lattice. International Journal of Solids and Structures 51, 3866-3877.

Khaled, S.A., Burley, J.C., Alexander, M.R., Yang, J., Roberts, C.J., 2015a. 3D printing of five-in-one dose combination polypill with defined immediate and sustained release profiles. J. Control. Release. 217, 308-314.

Khaled, S.A., Burley, J.C., Alexander, M.R., Yang, J., Roberts, C.J., 2015b. 3D printing of tablets containing multiple drugs with defined release profiles. Int. J. Pharm. 494, 643-650.

Kollamaram, G., Croker, D.M., Walker, G.M., Goyanes, A., Basit, A.W., Gaisford, S., 2018. Low temperature fused deposition modeling (FDM) 3D printing of thermolabile drugs. Int. J. Pharm. 545, 144-152.

Liu, F., Merchant, H.A., Kulkarni, R.P., Alkademi, M., Basit, A.W., 2011. Evolution of a physiological pH 6.8 bicarbonate buffer system: Application to the dissolution testing of enteric coated products. Eur. J. Pharm. Biopharm. 78, 151-157.

Martinez, P.R., Goyanes, A., Basit, A.W., Gaisford, S., 2017. Fabrication of drug-loaded hydrogels with stereolithographic 3D printing. Int. J. Pharm. 532, 313-317.

Melocchi, A., Parietti, F., Loreti, G., Maroni, A., Gazzaniga, A., Zema, L., 2015. 3D printing by fused deposition modeling (FDM) of a swellable/erodible capsular device for oral pulsatile release of drugs. J. Drug Deliv. Sci. Tec. 30, 360-367.

Melocchi, A., Parietti, F., Maroni, A., Foppoli, A., Gazzaniga, A., Zema, L., 2016. Hot-melt extruded filaments based on pharmaceutical grade polymers for 3D printing by fused deposition modeling. Int. J. Pharm. 509, 255-263.

Merchant, H.A., Frost, J., Basit, A.W., 2012. Apparatus and method for testing medicaments. PCT/GB2013/051145.

Merchant, H.A., Goyanes, A., Parashar, N., Basit, A.W., 2014. Predicting the gastrointestinal behaviour of modified-release products: Utility of a novel dynamic dissolution test apparatus involving the use of bicarbonate buffers. Int. J. Pharm. 475, 585-591.

Okwuosa, T.C., Stefaniak, D., Arafat, B., Isreb, A., Wan, K.-W., Alhnan, M.A., 2016. A lower temperature FDM 3D printing for the manufacture of patient-specific immediate release tablets. Pharm. Res. 33, 2704-2712.

Okwuosa, T.C., Soares, C., Gollwitzer, V., Habashy, R., Timmins, P., Alhnan, M.A., 2018. On demand manufacturing of patient-specific liquid capsules via co-ordinated 3D printing and liquid dispensing. Eur. J. Pharm. Sci. 118, 134-143.

Pharmaceutials, A. 2015. Manufactured Using 3D Printing, http://www.spritam.com/ -/hcp/zipdose-technology/manufactured-using-3d-printing., last accessed

Sadia, M., Arafat, B., Ahmed, W., Forbes, R.T., Alhnan, M.A., 2018. Channelled tablets: An innovative approach to accelerating drug release from 3D printed tablets. J. Control. Release. 269, 355-363.

Shirazi, S.F.S., Gharehkhani, S., Mehrali, M., Yarmand, H., Metselaar, H.S.C., Adib Kadri, N., Osman, N.A.A., 2015. A review on powder-based additive manufacturing for tissue engineering: selective laser sintering and inkjet 3D printing. Science and Technology of Advanced Materials 16, 033502.

Sibik, J., Sargent, M.J., Franklin, M., Zeitler, J.A., 2014. Crystallization and phase changes in paracetamol from the amorphous solid to the liquid phase. Mol. Pharm. 11, 1326-1334.

Trenfield, S.J., Awad, A., Goyanes, A., Gaisford, S., Basit, A.W., 2018. 3D Printing Pharmaceuticals: Drug Development to Frontline Care. Trends Pharmacol. Sci. 39, 440-451.

Varum, F.J., Merchant, H.A., Goyanes, A., Assi, P., Zboranova, V., Basit, A.W., 2014. Accelerating the dissolution of enteric coatings in the upper small intestine: evolution of a novel pH 5.6 bicarbonate buffer system to assess drug release. Int. J. Pharm. 468, 172-177.

Wang, J., Goyanes, A., Gaisford, S., Basit, A.W., 2016. Stereolithographic (SLA) 3D printing of oral modified-release dosage forms. Int. J. Pharm. 503, 207-212.

Yan, C., Hao, L., Hussein, A., Raymont, D., 2012. Evaluations of cellular lattice structures manufactured using selective laser melting. International Journal of Machine Tools and Manufacture 62, 32-38.

**Figure Captions**

**Figure 1.** 3D model of the A) cylindrical printlet and B) gyroid lattice printlet, from different angles.

**Figure 2**. Images of A) cylindrical 3D printed constructs and B) 3D printed gyroid lattice solid dosage forms of the different polymer formulations.

**Figure 3.** X-ray micro-CT images and cross-sections of A) cylindrical 3D printed structures and B) 3D printed gyroid lattice printlets.

**Figure 4.** SEM images of the cross sections of A) the cylindrical printlets and B) the gyroid lattice printlets.

**Figure 5.** DSC thermograms of pure paracetamol, individual polymers and mixtures prior to printing and the different printlet formulations.

**Figure 6.** X-ray powder diffractograms of pure paracetamol, mixtures before printing and 3D printed discs.

**Figure 7**. Drug dissolution profiles of A) the cylindrical and B) gyroid lattice constructs. The red line shows the pH values of the media in an acidic environment for the first 2 hours, followed by exposure to basic pH in a dynamic dissolution test.

**Figure 8**. Images of A) 3D model and B) 3D printed bi-layer construct.

**Figure 9**. Drug dissolution profiles of the bi-layer PEO constructs compared to the conventional and the gyroid lattice printlets. The red line shows the pH values of the media in an acidic environment for the first 2 hours, followed by exposure to basic pH in a dynamic dissolution test.

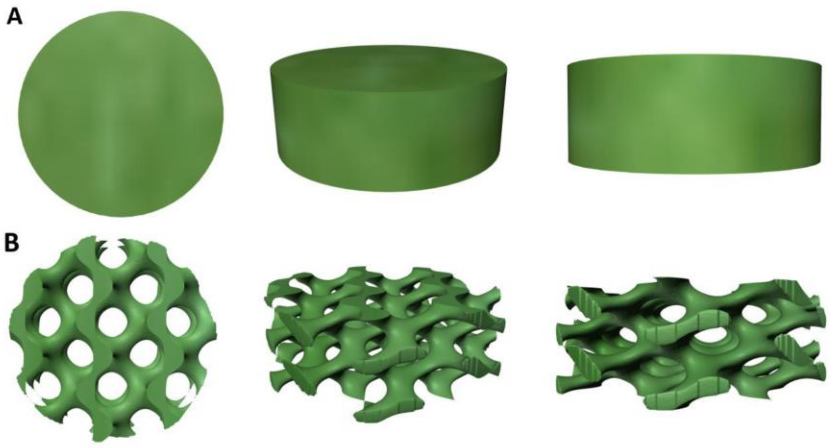
A
B

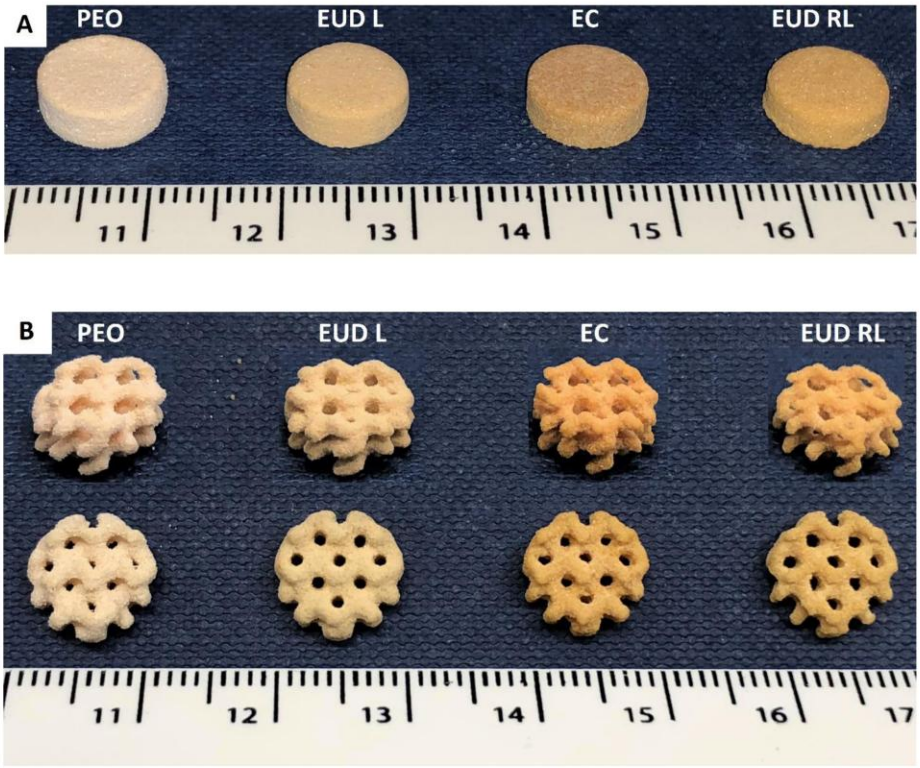
A
PEO
EUD L
EC
EUD RL
11
12
13
14
15
16
B
PEO
EUD L
EC
EUD RL
11
12
13
14
15
16
17

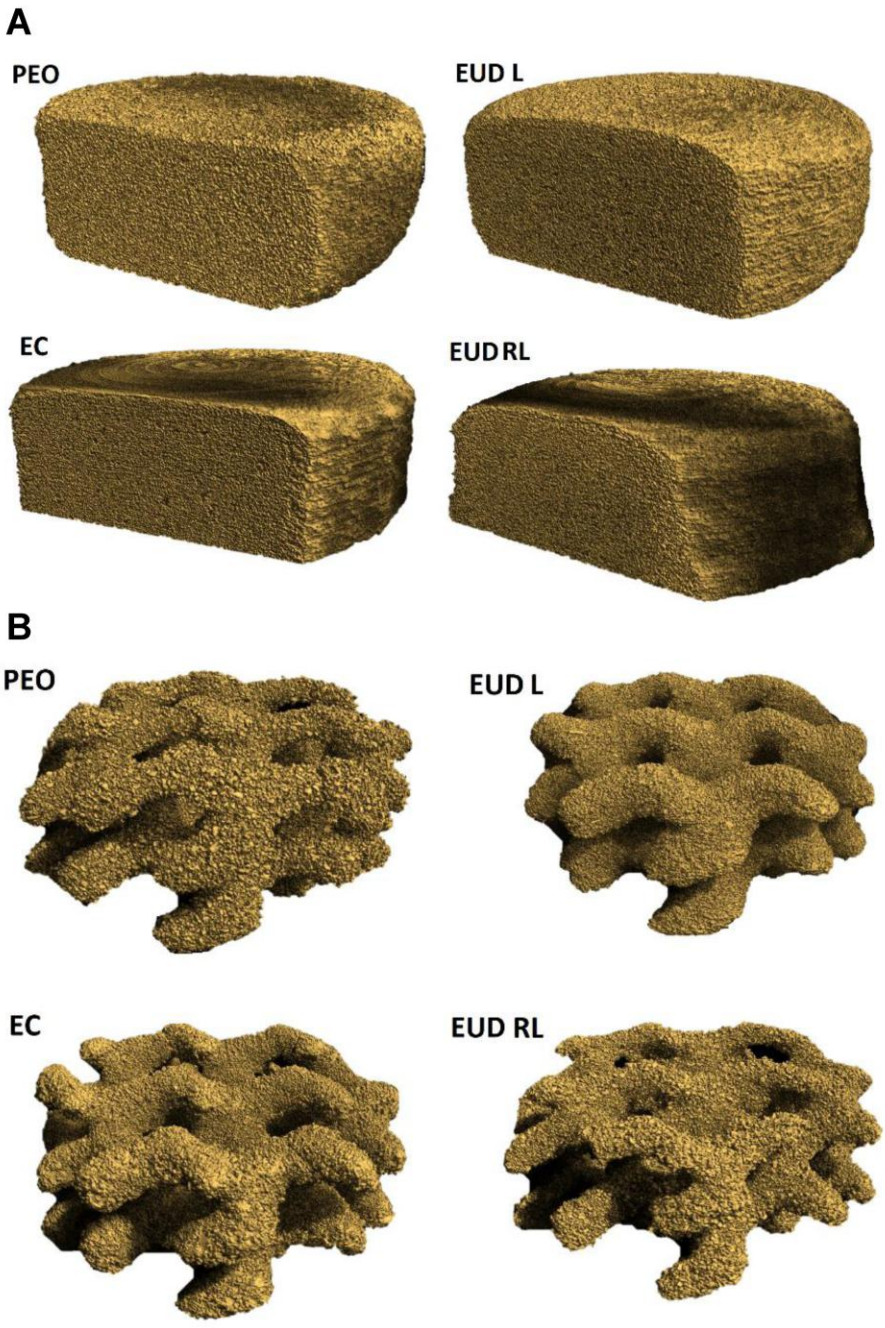
A
PEO
EUD L
EC
EUD RL
B
PEO
EUD L
EC
EUD RL

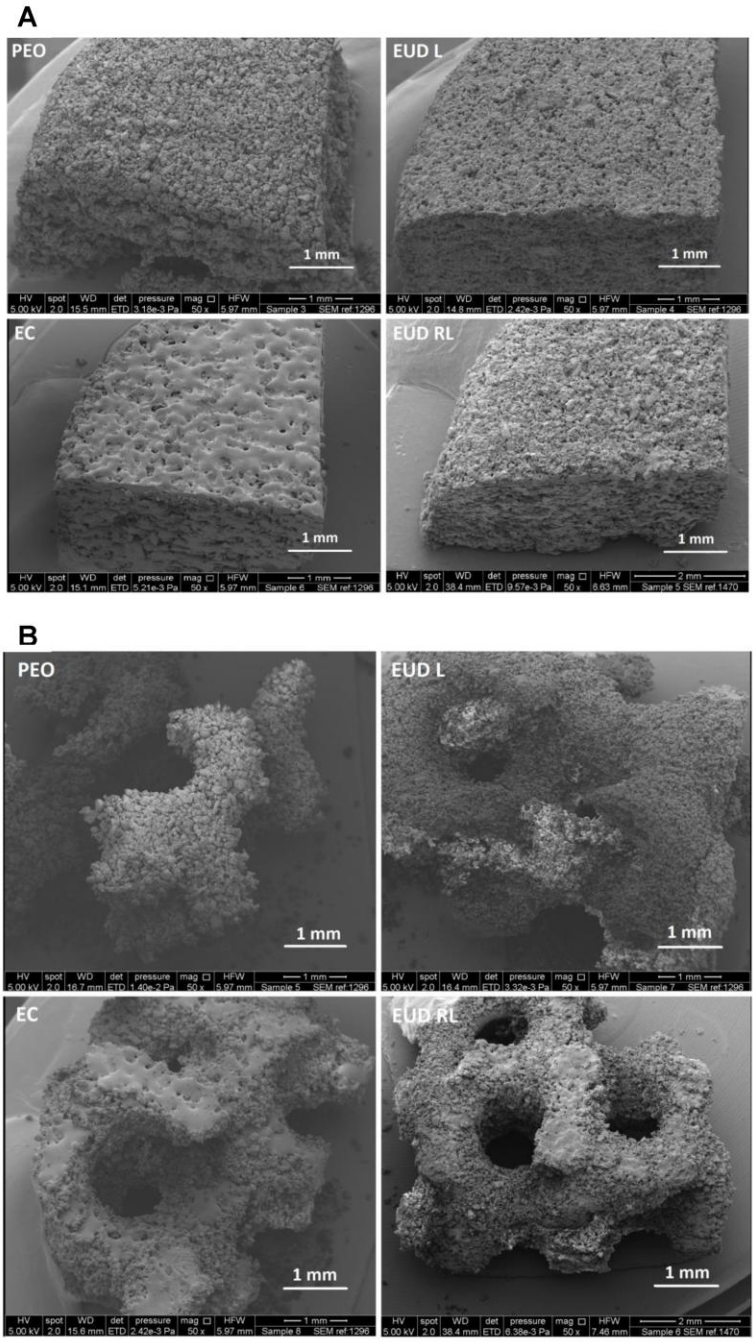

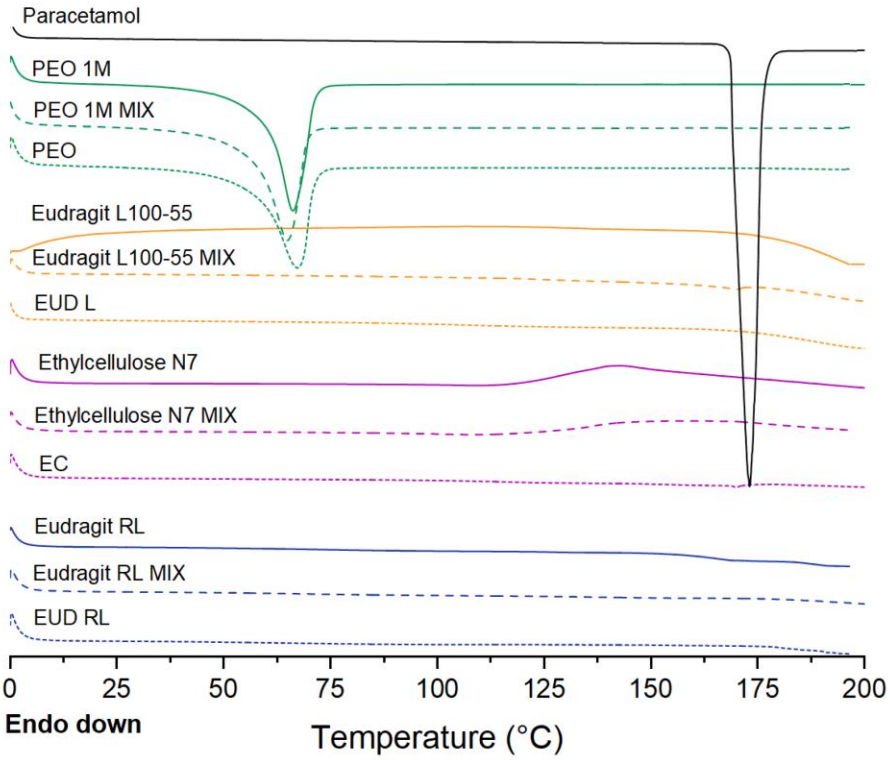

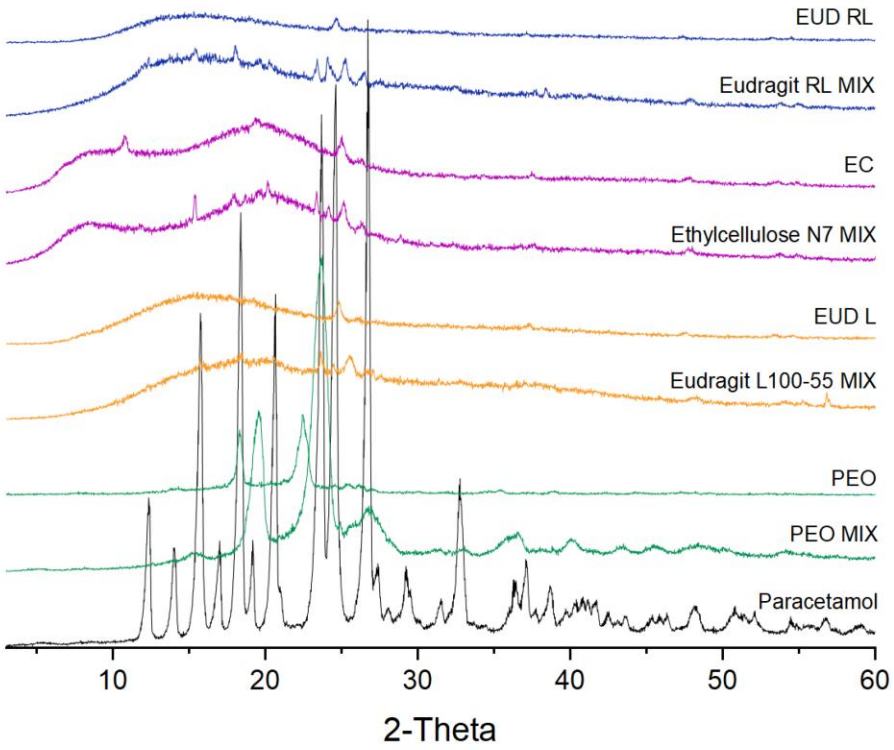

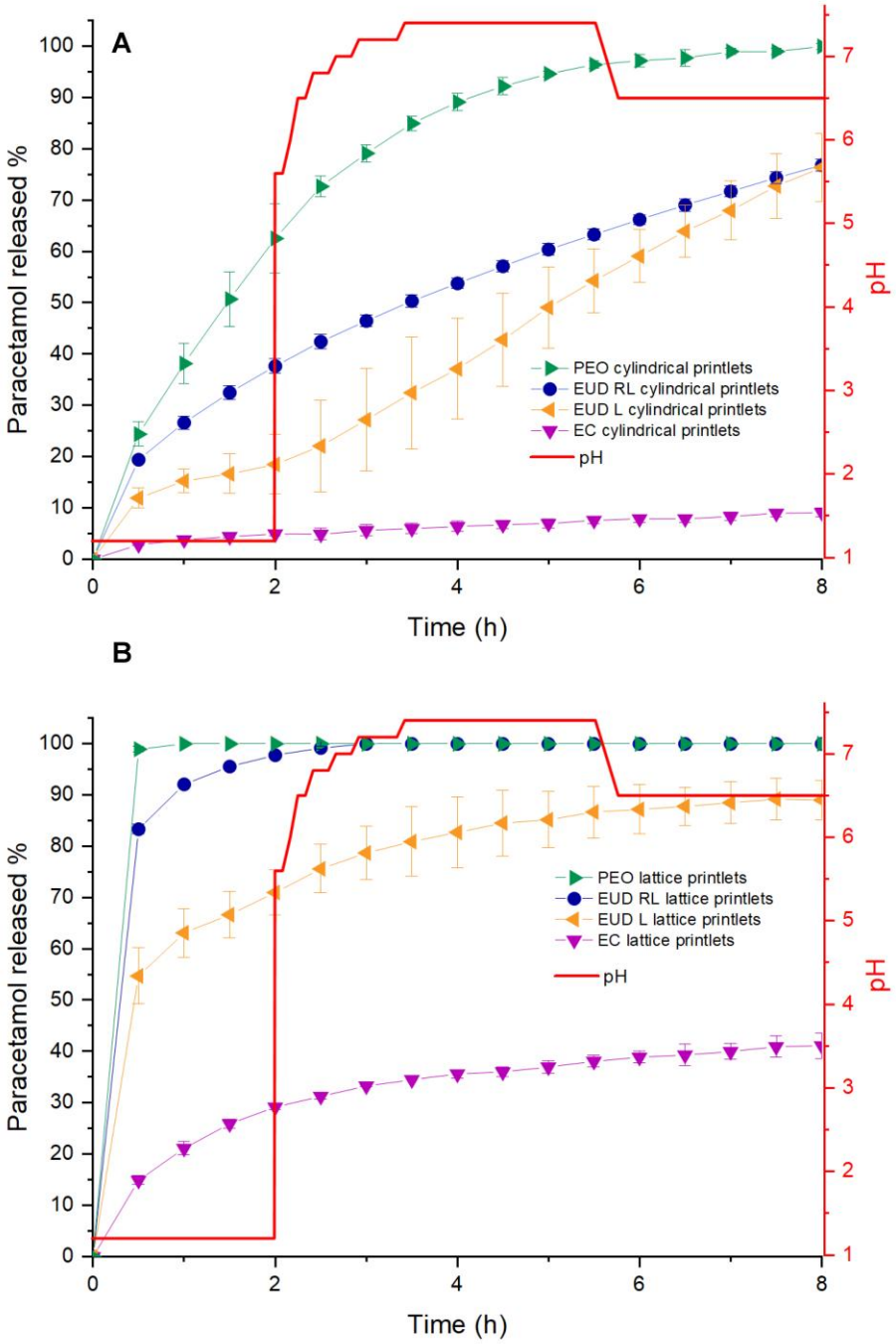

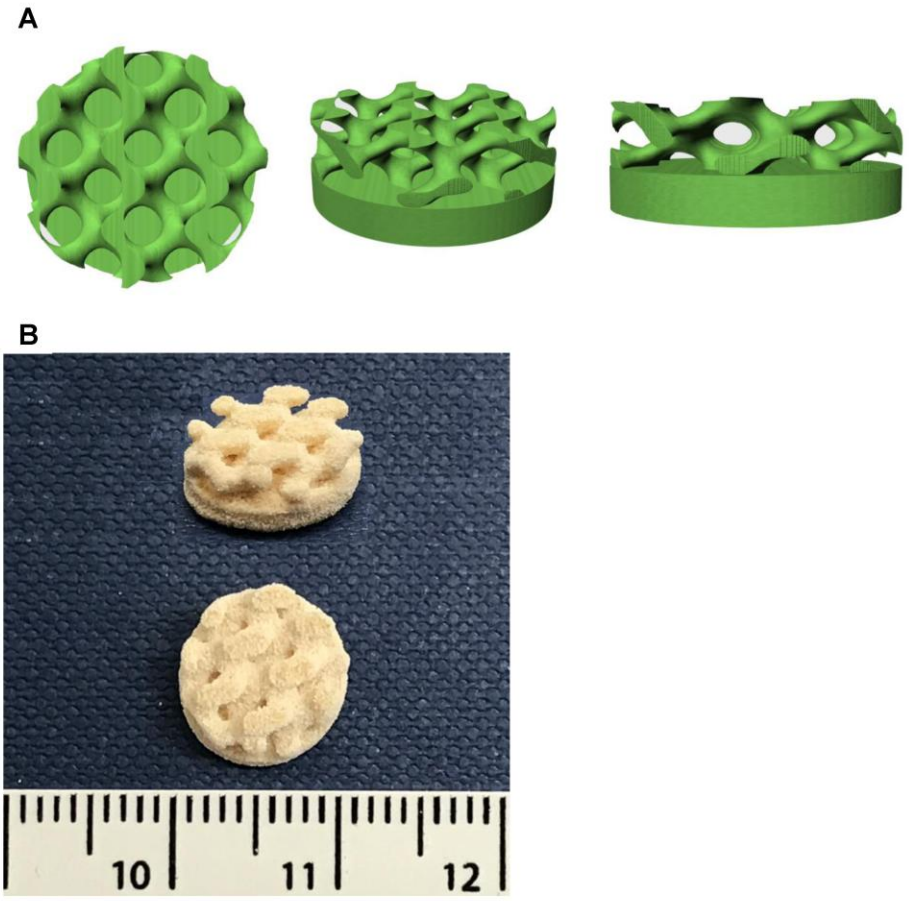
A
B
10
11
12

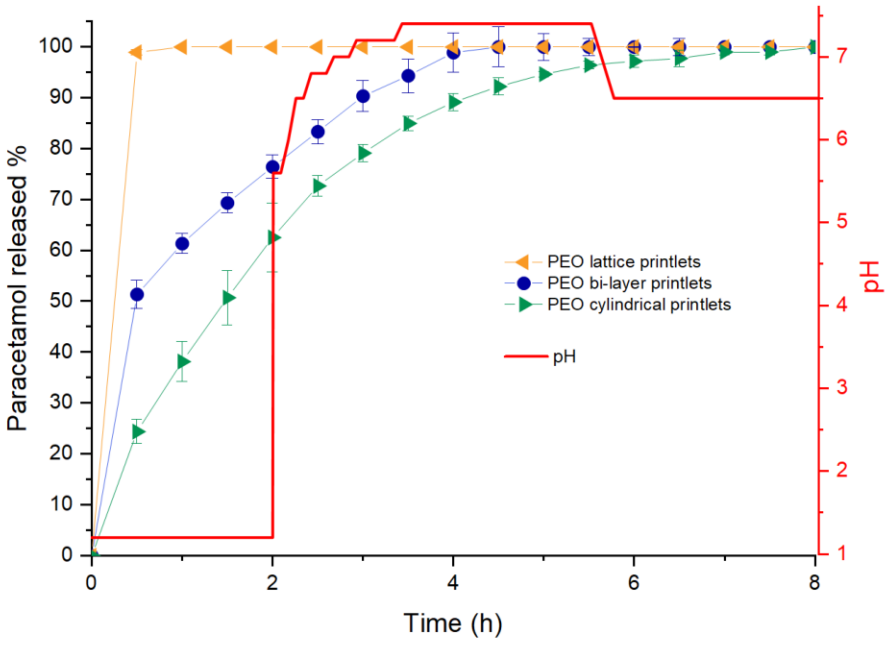

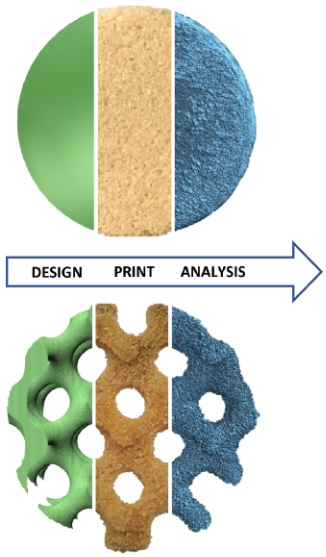


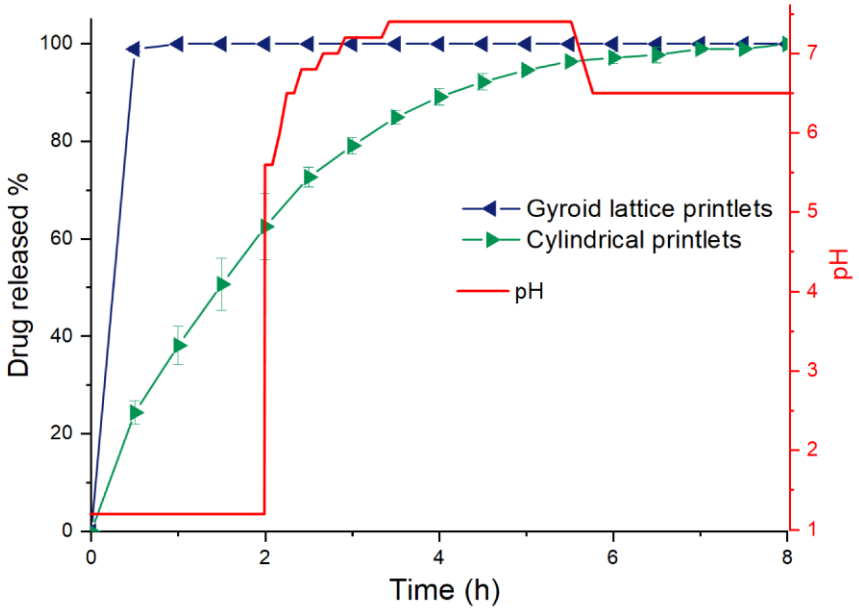

**Table 1.** Composition of the 3D printed formulations.

| Formulations* | % Content excipient | Chamber temperature (°C) | Surface temp (°C) |
|---|---|---|---|
| PEO | 92% Polyethylene oxide 1M | 35 | 50 |
| EUD L | 92% Eudragit L100-55 | 90 | 110 |
| EC | 92% Ethyl cellulose N7 | 100 | 120 |
| EUD RL | 92% Eudragit RL | 65 | 85 |

*All the formulations contain 3% w/w Candurin® Gold Sheen and are loaded with 5%

**Table 2.** Printlets characteristics

| Formulation | Cylindrical printlets | | | | Gyroid lattice printlets | | | | |
|---|---|---|---|---|---|---|---|---|---|
| | Weight (mg ± SD) | Drug content (% ± SD) | Porosity (% ± SD) | Breaking force (N ± SD) | Weight (mg ± SD) | Drug content (% ± SD) | Porosity including openings (% ± SD) | Porosity excluding openings (% ± SD) | Breaking force (N ± SD) |
| PEO | 172.8 ± 0.9 | 101.2 ± 0.8 | 28.0 ± 2.1 | -* | 62.7 ± 0.6 | 100.7 ± 0.6 | 61.7 ± 0.8 | 42.1 ± 2.7 | -* |
| EUD L | 192.1 ± 0.9 | 99.6 ± 1.2 | 26.9 ± 0.7 | 286.3 ± 2.5 | 94.1 ± 0.9 | 99.9 ± 1.4 | 40.78 ± 2.4 | 28.7 ± 4.2 | 15.5 ± 3.5 |
| EC | 248.9 ± 0.5 | 99.5 ± 0.4 | 3.9 ± 0.6 | 279 ± 2.7 | 120.3 ± 0.3 | 99.8 ± 0.8 | 45.1 ± 2.6 | 22.6 ± 4.1 | 15 ± 2.8 |
| EUD RL | 236.5 ± 0.5 | 100 ± 0.6 | 12.5 ± 1.0 | 281.7 ± 2.5 | 72.6 ± 0.4 | 99.5 ± 0.8 | 49.2 ± 3.7 | 32.8 ± 4.7 | -* |

* breaking force values could not be detected